Fibroblast growth factor 21 promotes bone loss by potentiating the effects of peroxisome proliferator-activated receptor γ

Wei Wei[a], Paul A. Dutchak[a,b], Xunde Wang[a], Xunshan Ding[a,b], Xueqian Wang[a], Angie L. Bookout[a,c,d], Regina Goetz[e], Moosa Mohammadi[e], Robert D. Gerard[b,d], Paul C. Dechow[f], David J. Mangelsdorf[a,g,1], Steven A. Kliewer[a,b], and Yihong Wan[a,1]

Departments of [a]Pharmacology and [b]Molecular Biology, [c]Division of Hypothalamic Research, [d]Department of Internal Medicine, and [g]Howard Hughes Medical Institute, University of Texas Southwestern Medical Center, Dallas, TX 75390; [e]Department of Pharmacology, New York University School of Medicine, New York, NY 10016; and [f]Department of Biomedical Sciences, Baylor College of Dentistry, Texas A & M University Health Sciences Center, Dallas, TX 75246

Contributed by David J. Mangelsdorf, January 15, 2012 (sent for review December 13, 2011)

The endocrine hormone fibroblast growth factor 21 (FGF21) is a powerful modulator of glucose and lipid metabolism and a promising drug for type 2 diabetes. Here we identify FGF21 as a potent regulator of skeletal homeostasis. Both genetic and pharmacologic FGF21 gain of function lead to a striking decrease in bone mass. In contrast, FGF21 loss of function leads to a reciprocal high-bone-mass phenotype. Mechanistically, FGF21 inhibits osteoblastogenesis and stimulates adipogenesis from bone marrow mesenchymal stem cells by potentiating the activity of peroxisome proliferator-activated receptor γ (PPAR-γ). Consequently, FGF21 deletion prevents the deleterious bone loss side effect of the PPAR-γ agonist rosiglitazone. Therefore, FGF21 is a critical rheostat for bone turnover and a key integrator of bone and energy metabolism. These results reveal that skeletal fragility may be an undesirable consequence of chronic FGF21 administration.

bone metabolism | osteoblast | thiazolidinediones | adipocyte | nuclear receptor

Bone is a dynamic tissue that constantly remodels by balancing osteoblast-mediated bone formation and osteoclast-mediated bone resorption. Under physiological conditions, formation and resorption are tightly coupled, thereby maintaining skeletal homeostasis. Under pathological conditions such as osteoporosis or bone metastasis of cancer, the simultaneously decreased formation and increased resorption lead to the uncoupling of remodeling and bone loss (1–3). Osteoblasts are differentiated from bone marrow mesenchymal stem cells (MSCs), which can also differentiate into adipocytes, depending on both extracellular milieu and intracellular signaling (4–8). In contrast, osteoclasts are differentiated from macrophage precursors in the hematopoietic lineage in response to the cytokine Receptor Activator of NF-κB Ligand (RANKL), depending on the ratio of RANKL to osteoprotegerin (OPG), a RANKL decoy receptor that inhibits osteoclast differentiation (9).

Fibroblast growth factor 21 (FGF21) is an atypical member of the FGF family that functions as an endocrine hormone (10, 11). It is a powerful regulator of glucose and lipid metabolism. Physiologically, FGF21 expression is induced both in the liver by prolonged fasting through PPAR-α activation (12–14) and in the white adipose tissue by feeding through PPAR-γ activation (15–18). Pharmacologically, administration of recombinant FGF21 protein to diabetic mice and rhesus monkeys strongly enhances insulin sensitivity, decreases plasma glucose and triglyceride, and reduces body weight (19–23). Hence, FGF21 is a potential drug for the treatment of obesity and diabetes that is currently in clinical trials. However, it is unknown whether FGF21 regulates bone mass. This question is clinically important in light of the already increased skeletal fragility in diabetic patients (24, 25) and the reported bone-loss side effects of the current antidiabetic thiazolidinedione (TZD) drugs such as rosiglitazone, a synthetic PPAR-γ agonist (24, 26–29). Here we demonstrate that FGF21 is a potent negative regulator of bone, both physiologically and pharmacologically. These findings identify FGF21 as a critical, yet previously unrecognized, regulator of skeletal homeostasis and a key integrator of bone and energy metabolism.

Results and Discussion

Genetic FGF21 Gain of Function Decreases Bone Mass. To examine the consequences of chronic FGF21 exposure on bone, we used FGF21-transgenic (Tg) mice, in which circulating FGF21 concentrations are approximately fivefold higher than in fasted mice (13, 30). Micro-computed tomography (μCT) imaging of the tibiae demonstrated that the FGF21-Tg mice had a striking decrease in trabecular bone compared with the wild-type (WT) controls (Fig. 1*A*). Quantification of bone parameters showed that the FGF21-Tg mice had significant reductions in the bone volume (BV)/tissue volume (TV) ratio (BV fraction, −51%), bone surface (BS; −55%), trabecular number (Tb.N; −27%), and trabecular thickness (Tb.Th; −36%), along with significant increases in BS/BV ratio (+60%) and trabecular separation (Tb.Sp; +63%) (Fig. 1*B*). Both the apparent density (tissue mineral density; TMD) and material density (bone mineral density; BMD) were decreased in the FGF21-Tg mice (Fig. 1*C*). BV/TV and BMD of cortical bones (Fig. 1*D*) and whole tibiae (Fig. S1*A*) were also significantly reduced.

To determine whether the low-bone-mass phenotype was caused by decreased bone formation and/or increased bone resorption, we measured bone markers by ELISA. The bone formation marker N-terminal propeptide of type I procollagen (PINP) was 40% lower (Fig. 1*E*), whereas the bone resorption marker C-terminal telopeptide fragments of the type I collagen (CTX-1) was 122% higher in the FGF21-Tg mice (Fig. 1*F*). Static bone histomorphometry studies showed that osteoblast number and surface were significantly lower (Fig. 1*G*), whereas osteoclast number and surface were significantly higher (Fig. 1*H*). Interestingly, the number and area of bone marrow adipocytes were markedly increased in the FGF21-Tg mice (Fig. 1 *I* and *J*). Dynamic histomorphometry analysis using double calcein labeling showed that the FGF21-Tg mice exhibited a significantly lower bone formation rate (BFR/BS; +98%), mineral apposition rate (MAR; +38%), and mineralizing surface (MS)/BS ratio (MS/BS; +36%) (Fig. 1 *K* and *L*). Analysis of mRNA expression in tibiae confirmed that osteoblast-specific genes (osterix and osteocalcin) were reduced, whereas adipocyte-spe-

Author contributions: D.J.M., S.A.K., and Y.W. designed research; W.W., P.A.D., Xunde Wang, X.D., Xueqian Wang, and A.L.B. performed research; R.G., M.M., R.D.G., and P.C.D. contributed reagents/analytic tools; W.W., D.J.M., S.A.K., and Y.W. analyzed data; and D.J.M., S.A.K., and Y.W. wrote the paper.

The authors declare no conflict of interest.

[1]To whom correspondence may be addressed. E-mail: davo.mango@utsouthwestern.edu or yihong.wan@utsouthwestern.edu.

This article contains supporting information online at www.pnas.org/lookup/suppl/doi:10.1073/pnas.1200797109/-/DCSupplemental.

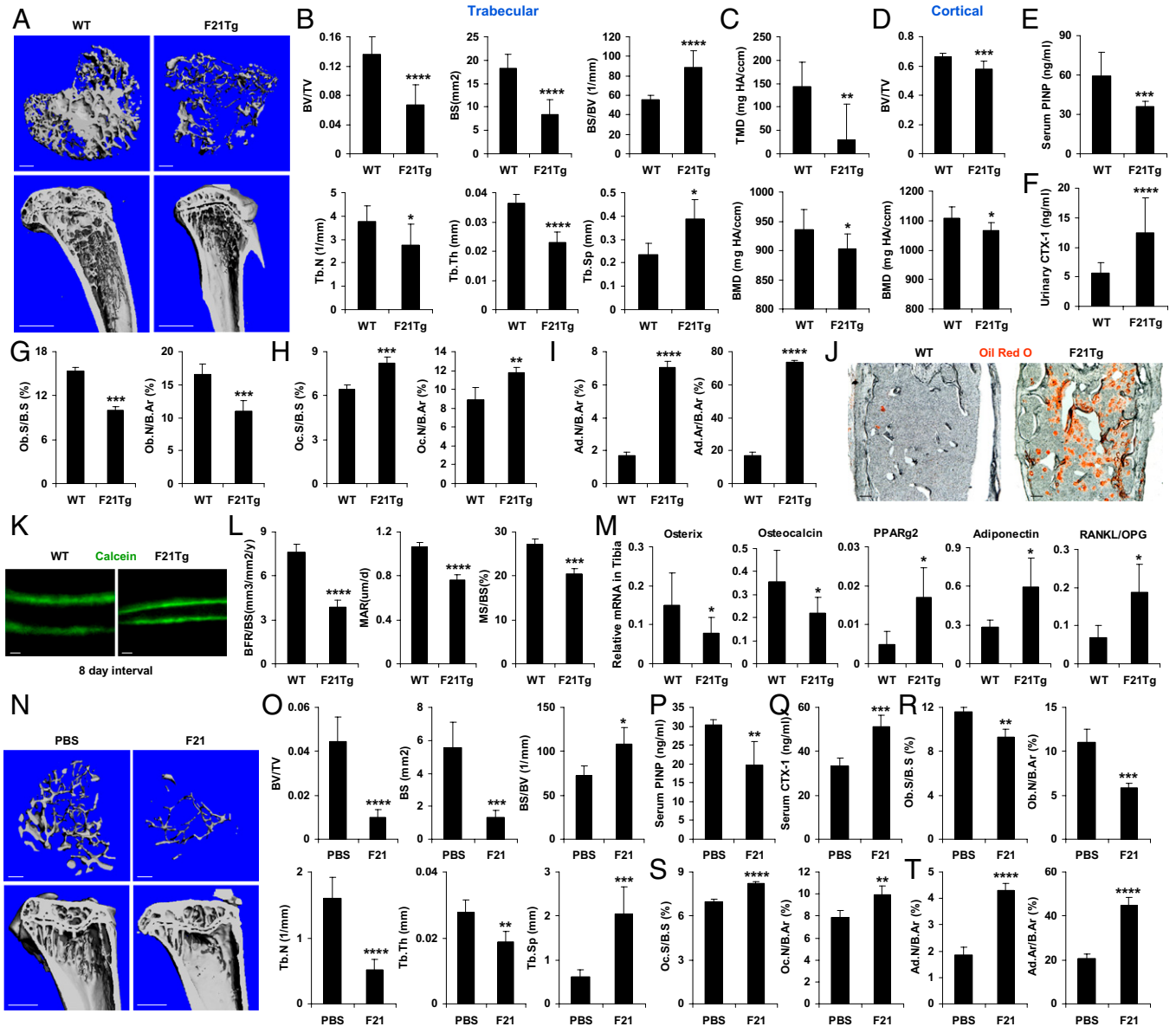

Fig. 1. Genetic and pharmacological FGF21 gain of function decreases bone mass. (*A* and *B*) FGF21-Tg mice displayed a low-bone-mass phenotype. Tibiae from FGF21-Tg or WT littermate controls (6 mo old, male, $n = 7$) were analyzed by μCT. (*A*) Representative images of the trabecular bone of the tibial metaphysis (*Upper*) and the entire proximal tibia (*Lower*). (Scale bars: *Upper*, 10 μm; *Lower*, 1 mm). (*B*) Quantification of trabecular bone volume and architecture. (*C*) Trabecular bone apparent density and material density were decreased in FGF21-Tg mice. (*Upper*) TMD. (*Lower*) BMD. (*D*) Cortical BV/TV (*Upper*) and BMD (*Lower*) were decreased. (*E*) Serum PINP was decreased (6 mo old, male, $n = 8$). (*F*) Urinary CTX-1 was increased (6 mo old, male, $n = 15$). (*G–J*) Static bone histomorphometry showed decreased osteoblasts but increased osteoclasts and adipocytes in the femurs of FGF21-Tg mice (6 mo old, male, $n = 6$). (*G*) Osteoblast surface (Ob.S/BS) and number (Ob.N/B.Ar). B.Ar, bone area. (*H*) Osteoclast surface (Oc.S/BS) and number (Oc.N/B.Ar). (*I*) Adipocyte number (Ad.N/B.Ar) and area (Ad.Ar/B.Ar). (*J*) Oil Red O (ORO)-stained femoral sections. Adipocytes were ORO$^+$ (red) cells. (Scale bar, 100 μm.) (*K* and *L*) Dynamic bone histomorphometry (2 mo old, male, $n = 6$). Calcein was injected 2 and 10 d before bone collection. (*K*) Representative images of the femoral sections. (Scale bars, 10 μm.) (*L*) Quantification of BFR/BS, MAR, and MS/BS. (*M*) Expression of marker genes for osteoblasts (osterix and osteocalcin), adipocytes (PPAR-γ2 and adiponectin), and RANKL/OPG ratio in the tibiae of FGF21-Tg mice and WT controls ($n = 4$). (*N–T*) Pharmacological FGF21 treatment induces bone loss. WT mice (6 mo old at end point, male, $n = 4$) were fed a high-fat diet for 4 mo and injected with FGF21 (1 mg·kg^{-1}·d^{-1}) or PBS control daily during the last 2 wk. (*N* and *O*) μCT of the tibiae showed that FGF21 caused a trabecular bone loss. (*N*) Representative images of the trabecular bone of the tibial metaphysis (*Upper*) and the entire proximal tibia (*Lower*). (Scale bars: *Upper,* 10 μm; *Lower*, 1 mm.) (*O*) Trabecular bone volume and architecture. (*P*) Serum PINP. (*Q*) Serum CTX-1. (*R*) Osteoblast surface/number. (*S*) Osteoclast surface/number. (*T*) Adipocyte number/area. *$P < 0.05$; **$P < 0.01$; ***$P < 0.005$; ****$P < 0.001$.

cific genes (PPAR-γ2 and adiponectin) were elevated (Fig. 1*M*). In addition, the mRNA ratio of RANKL/OPG was elevated (Fig. 1*M*), suggesting that the increased bone resorption may result from increased RANKL availability. These results show that the low bone mass in the FGF21-Tg mice was caused by a combination of decreased bone formation and increased bone resorption.

Pharmacological FGF21 Treatment Induces Severe Bone Loss. Because FGF21 is a promising diabetes drug currently in clinical trials, we investigated whether shorter-term FGF21 treatment also caused bone loss in diet-induced obese (DIO) mice. WT mice were fed a high-fat diet for 4 mo and injected with recombinant FGF21 (1 mg·kg^{-1}·d^{-1}) or PBS control during the last 2 wk. μCT imaging of the tibiae showed that FGF21 treatment caused marked

trabecular bone loss (Fig. 1*N*) with a significant reduction in BV/TV (−78%), BS (−77%), Tb.N (−68%), and Tb.Th (−32%), accompanied by a significant increase in BS/BV (+48%) and Tb.Sp (+3.3 fold) (Fig. 1*O*). ELISA analyses showed that the FGF21-induced bone loss was caused by a combination of decreased bone formation (−35% in PINP) (Fig. 1*P*) and increased bone resorption (+54% in CTX-1) (Fig. 1*Q*). Histomorphometry showed that FGF21 treatment led to significantly reduced osteoblast number and surface (Fig. 1*R*), increased osteoclast number and surface (Fig. 1*S*), and increased bone marrow adipocyte number and area (Fig. 1*T*). Consistent with the recombinant FGF21 studies, adenovirus-mediated FGF21 overexpression caused significant bone loss after 2 wk in DIO mice (Fig. S2) and after 4 wk in lean mice (Fig. S3). Thus, pharmacologic FGF21 administration causes severe bone loss in adult animals.

Genetic FGF21 Loss of Function Increases Bone Mass. To determine whether FGF21 is required for normal bone homeostasis, we analyzed FGF21-knockout (KO) mice (31). μCT imaging of tibiae showed that FGF21-KO mice developed a high-bone-mass phenotype with more trabecular bone than the WT controls (Fig. 2*A*). FGF21-KO mice showed significantly greater BV/TV (+87%), BS (+101%), Tb.N (+64%), and connectivity density (Conn. D., +241%), accompanied by significantly decreased Tb.Sp (−44%) (Fig. 2*B*). BV/TV of cortical bones (Fig. 2*C*) and whole tibiae (Fig. S1*B*) was also significantly increased. The bone formation marker PINP was 152% higher (Fig. 2*D*), whereas the bone resorption marker CTX-1 was 45% lower in the FGF21-KO mice (Fig. 2*E*). As is often seen in mice with osteoclast defects, the FGF21-KO mice also exhibited extramedullary hematopoiesis in the spleen, evidenced by increased spleen/body weight ratio (Fig. 2*F Left*) with unaltered body weight (Fig. 2*F Right*). The mRNA ratio of RANKL/OPG was lower in FGF21-KO mice (Fig. 2*G*), suggesting that the decreased bone resorption may result from reduced RANKL availability. Dynamic histomorphometry analysis showed that the FGF21-KO mice had a significantly higher BFR/BS (+98%), MAR (+38%), and MS/BS (+36%) (Fig. 2 *H* and *I*). Static histomorphometry analysis showed that osteoblast number and surface were significantly higher (Fig. 2*J*), whereas osteoclast number and surface were lower (Fig. 2*K*), in the FGF21-KO mice. Interestingly, the number and area of bone marrow adipocytes were also decreased in the FGF21-KO mice (Fig. 2 *L* and *M*). Together, these results show that the high-bone-mass phenotype in the FGF21-KO mice is caused by a combination of increased bone formation and decreased bone resorption. These findings further reveal FGF21 to be a physiologically relevant regulator of skeletal homeostasis.

FGF21 Inhibits Osteoblastogenesis but Enhances Marrow Adipogenesis in Synergy with Rosiglitazone. The negative correlation between the number of osteoblasts and adipocytes in bone marrow in both FGF21-Tg and -KO mice suggested that FGF21 might promote adipogenesis to the exclusion of osteoblastogenesis. In this regard, we have shown that FGF21 activates PPAR-γ transcriptional activity in white adipose tissue by inhibiting its sumoylation at K107, and, as a consequence, the insulin-sensitizing effects of TZDs are compromised in the absence of FGF21 (15). Together, these findings suggest that a similar interplay between FGF21 and PPAR-γ activity may exist in bone. To test whether FGF21 alters the adipocyte:osteoblast balance, we performed ex vivo bone marrow differentiation assays under conditions that favored either adipocyte or osteoblast formation. FGF21 treatment significantly increased the differentiation of marrow MSCs to adipocytes as measured by

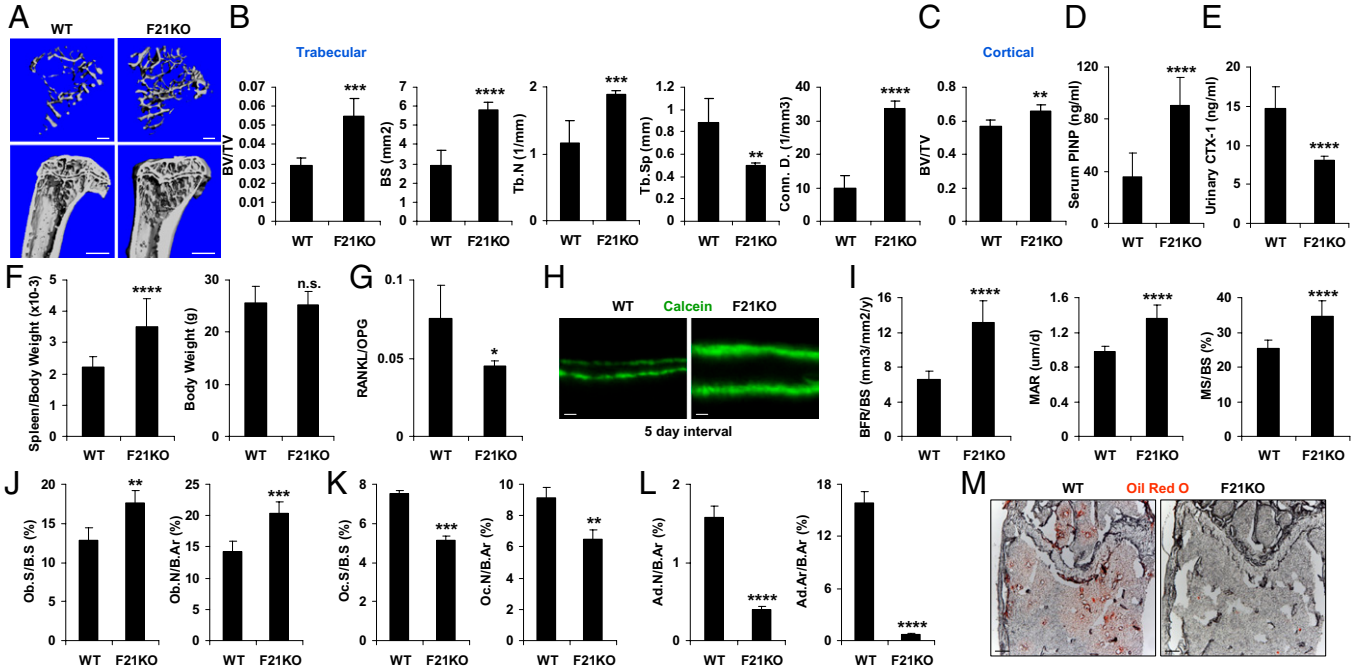

Fig. 2. Genetic FGF21 loss of function increases bone mass. (*A–C*) FGF21-KO mice displayed a high-bone-mass phenotype. Tibiae from FGF21-KO or WT controls (4 mo old, male, $n = 4$) were analyzed by μCT. (*A*) Representative images of the trabecular bone of the tibial metaphysis (*Upper*) and the entire proximal tibia (*Lower*). (Scale bars: *Upper*, 10 μm; *Lower*, 1 mm.) (*B*) Quantification of trabecular bone volume and architecture. (*C*) Cortical BV/TV was increased. (*D*) Serum PINP was increased (4 mo old, male, $n = 7$). (*E*) Urinary CTX-1 was decreased (4 mo old, male, $n = 7$). (*F*) FGF21-KO mice had a greater spleen/body weight ratio (*Left*) with unaltered body weight (*Right*) (6 mo old, male, $n = 20$). (*G*) Expression of RANKL/OPG mRNA ratio in the tibiae ($n = 4$). (*H* and *I*) Dynamic bone histomorphometry (2 mo old, male, $n = 6$). Calcein was injected 2 and 7 d before bone collection. (*H*) Representative images of the femoral sections. (Scale bars, 10 μm.) (*I*) Quantification of BFR/BS, MAR, and MS/BS. (*J–M*) Static bone histomorphometry showed increased osteoblasts but decreased osteoclasts and adipocytes in the femurs of FGF21-KO mice (6 mo old, male, $n = 6$). (*J*) Osteoblast surface and number. (*K*) Osteoclast surface and number. (*L*) Adipocyte number and area. (*M*) ORO-stained femoral sections. Adipocytes were ORO$^+$ (red) cells. (Scale bars, 100 μm.) $^*P < 0.05$; $^{**}P < 0.01$; $^{***}P < 0.005$; $^{****}P < 0.001$; n.s. nonsignificant ($P > 0.05$).

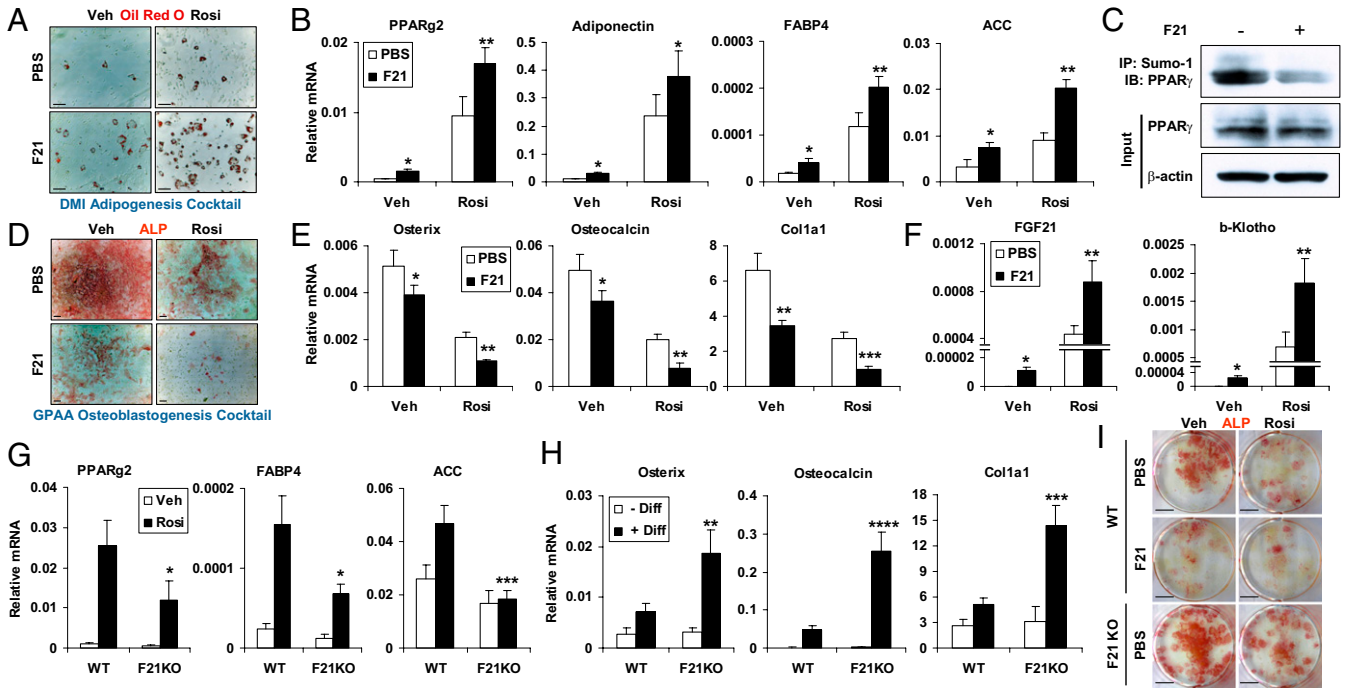

Fig. 3. FGF21 enhances adipogenesis and inhibits osteoblastogenesis in synergy with rosiglitazone. (*A* and *B*) Bone marrow cells from WT mice were differentiated into adipocytes ex vivo by using DMI (dexamethasone, IBMX, insulin) mixture in the presence or absence of FGF21 (0.2 μg/mL) and/or rosiglitazone (1 μM). (*A*) ORO-stained adipocyte differentiation culture. Mature adipocytes were ORO$^+$ (red) cells. (Scale bars, 25 μm.) (*B*) Expression of adipocyte-specific genes (n = 3). (*C*) Immunoprecipitation analysis of the effects of FGF21 treatment (0.2 μg/mL, 4 h) on the levels of sumoylated-PPAR-γ in adipocytes differentiated from FGF21-KO bone marrow cells. IP, immunoprecipitation; IB, immunoblot. (*D* and *E*) Bone marrow cells from WT mice were differentiated into osteoblasts ex vivo by using GPAA (β-glycerophosphate, ascorbic acid) mixture in the presence or absence of FGF21 (0.2 μg/mL) and/or rosiglitazone (1 μM). (*D*) ALP-stained osteoblast differentiation cultures. Mature osteoblasts were ALP$^+$ (red) cells. (Scale bars, 100 μm.) (*E*) Expression of osteoblast-specific genes (n = 3). (*F*) Expression of FGF21 and β-klotho in the adipocyte differentiation culture (n = 3). The P values in *B*, *E*, and *F* compare FGF21 and PBS treatments. (*G*) Expression of adipocyte-specific genes in the adipocyte differentiation cultures from WT or FGF21-KO mice with or without rosiglitazone (1 μM; n = 3). (*H*) Expression of osteoblast-specific genes in the bone marrow cultures from WT or FGF21-KO mice with or without osteoblast differentiation mixture (diff) (n = 3). The P values in *G* and *H* compare FGF21-KO with WT controls under the same treatment condition. (*I*) ALP-stained osteoblast differentiation cultures from WT or FGF21-KO mice, with or without FGF21 (0.2 μg/mL) and/or rosiglitazone (1 μM). (Scale bars, 0.5 cm.) *P < 0.05; **P < 0.01; ***P < 0.005; ****P < 0.001.

Oil Red O (ORO) staining and adipocyte-specific gene expression (Fig. 3 *A* and *B*). The effects of FGF21 were potentiated by inclusion of the PPAR-γ agonist rosiglitazone in the differentiation mixture, because the induction of adipocyte-specific genes by FGF21 and rosiglitazone cotreatment was higher than the additive induction by FGF21 or rosiglitazone alone (Fig. 3 *A* and *B*). Treating bone marrow adipocytes with FGF21 for 4 h caused a marked decrease in sumoylated PPAR-γ without affecting total PPAR-γ levels (Fig. 3*C*), in keeping with the notion that FGF21 potentiates PPAR-γ activity (15). In osteoblast differentiation assays, FGF21 inhibited the development of alkaline phosphatase-positive (ALP$^+$) cells and osteoblast-specific gene expression (Fig. 3 *D* and *E*). Once again, these effects were potentiated by inclusion of rosiglitazone (Fig. 3 *D* and *E*). Thus, FGF21 favors the differentiation of adipocytes over osteoblasts.

In adipocyte differentiation assays, the combination of FGF21 and rosiglitazone induced expression of the endogenous *Fgf21* gene and the FGF21 coreceptor β-*klotho* (Fig. 3*F*). These findings suggest the existence of a feed-forward PPAR-γ–FGF21 regulatory pathway and led us to examine the consequences of eliminating FGF21 in the MSC differentiation assays. In adipocyte differentiation assays, rosiglitazone's effect on adipocyte-specific gene expression was significantly attenuated in FGF21-KO cells (Fig. 3*G*). In contrast, in osteoblast differentiation assays, the induction of osteoblast-specific genes and formation of ALP$^+$ colonies was enhanced in FGF21-KO cultures compared with WT cultures (Fig. 3 *H* and *I*). These results highlight the importance of endogenous FGF21 in determining the ratio of osteoblasts to adipocytes.

FGF21 Does Not Directly Affect Osteoclastogenesis but Alters RANKL/OPG Ratio. Our findings of increased osteoclast number and bone resorption in the FGF21-Tg mice (Fig. 1) suggested that FGF21 might stimulate osteoclastogenesis. However, when treated with the same concentration of RANKL in vitro, hematopoietic progenitors from FGF21-Tg or -KO mice underwent normal osteoclast differentiation compared with the WT mice (Fig. S4 *A* and *B*). Moreover, in vitro FGF21 treatment had no effect on either RANKL-induced or rosiglitazone-stimulated osteoclast differentiation (Fig. S4*C*). Consistent with these findings, β-*klotho* was neither expressed nor induced by rosiglitazone in macrophage precursors and mature osteoclasts (data not shown). These results suggest that the higher bone resorption caused by FGF21 in vivo is likely mediated by indirect effects from other cell types or secreted factors that were absent in the ex vivo differentiation cultures. Although further studies are needed to address the full mechanism of FGF21 action on bone resorption, our findings that the RANKL/OPG ratio was higher in FGF21-Tg and lower in FGF21-KO mice (Figs. 1*M* and 2*G*) indicate that altered RANKL availability in vivo contributed, at least in part, to the changes in osteoclast number and bone resorption in these mice. In light of the recent studies on the role of osteocyte in RANKL production and bone remodeling (32, 33), our results suggest that osteocytes may also be targets of FGF21.

FGF21 Deletion Confers Resistance to Rosiglitazone-Induced Bone Loss. Human clinical trials have shown that long-term use of TZDs such as rosiglitazone increases fracture rates among diabetic patients (24, 26–29). Moreover, TZDs cause bone loss in

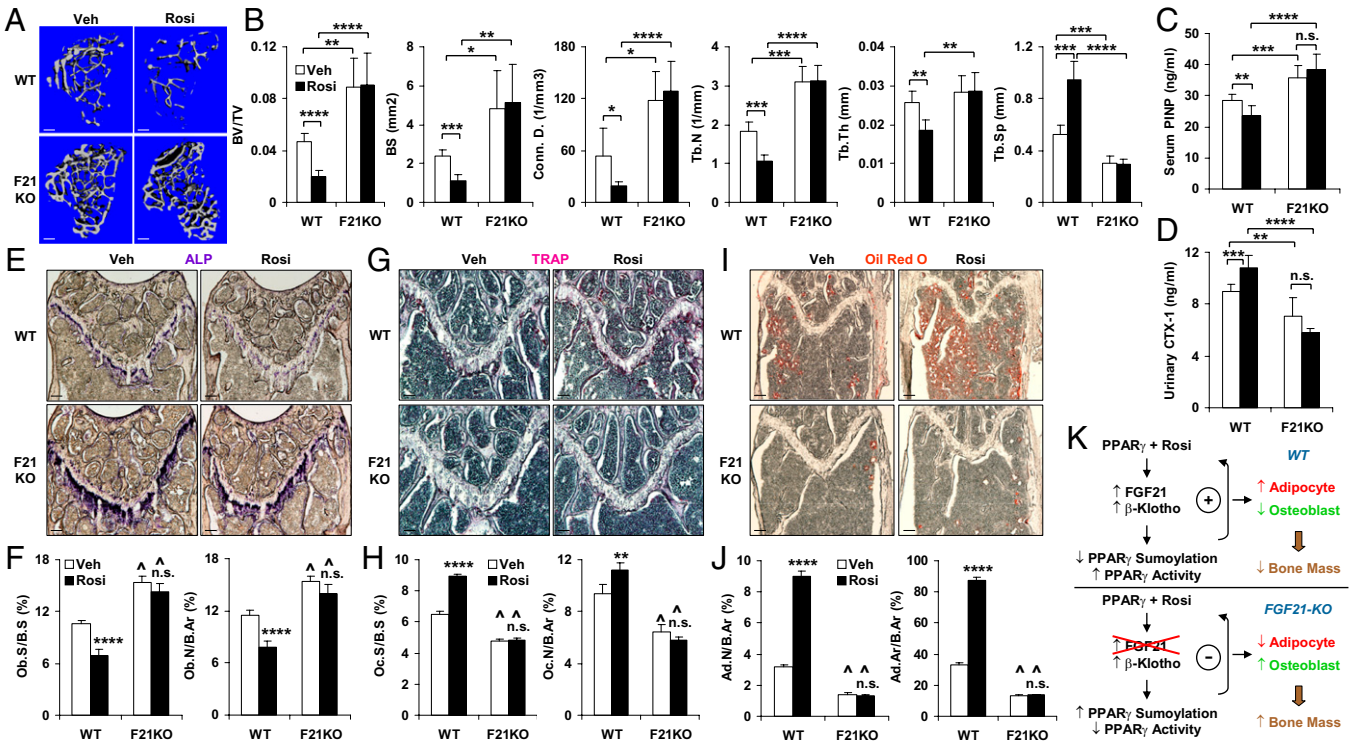

Fig. 4. FGF21 deletion confers resistance to rosiglitazone-induced bone loss. WT or FGF21-KO mice (6 mo old at end point, male) were fed a high-fat diet for 10 wk and treated with rosiglitazone (10 $mg \cdot kg^{-1} \cdot d^{-1}$) or vehicle control daily by oral gavage during the last 2 wk. (*A* and *B*) μCT of the tibiae showed that rosiglitazone-induced bone loss was abolished in the FGF21-KO mice. (*A*) Representative images of the trabecular bone of the tibial metaphysis. (Scale bars, 10 μm.) (*B*) Quantification of trabecular bone volume and architecture ($n = 4$). (*C*) Serum PINP ($n = 6$). (*D*) Urinary CTX-1 ($n = 6$). (*E*–*J*) Bone histomorphometry ($n = 6$). (Scale bars, 100 μm.) (*E*) ALP-stained femoral sections. Osteoblasts were ALP^+ (blue) cells. (*F*) Osteoblast surface and number. (*G*) TRAP-stained femoral sections. Osteoclasts were multinucleated $TRAP^+$ (purple) cells. (*H*) Osteoclast surface and number. (*I*) ORO-stained femoral sections. Adipocytes were ORO^+ (red) cells. (*J*) Adipocyte number and area. For the *P* values in *F*, *H*, and *J*, * compares rosiglitazone and vehicle treatment in the same group, and ^ indicates $P < 0.001$ by comparing F21KO with WT under the same treatment condition. (*K*) A diagram illustrating the feed-forward mechanism for how FGF21 mediates rosiglitazone-induced bone loss by enhancing PPAR-γ activity in the bone marrow mesenchymal lineages to promote adipogenesis and suppress osteoblastogenesis. $*P < 0.05$; $**P < 0.01$; $***P < 0.005$; $****P < 0.001$; n.s. nonsignificant ($P > 0.05$).

mice and rats because of the simultaneously decreased bone formation and increased bone resorption (7, 34–39). Thus, we next investigated whether FGF21 contributes to TZD-induced bone loss in obese mice. WT or FGF21-KO mice were fed a high-fat diet for 10 wk and treated with rosiglitazone (10 $mg \cdot kg^{-1} \cdot d^{-1}$) or vehicle control during the last 2 wk. μCT imaging of the tibiae demonstrated that in WT mice, rosiglitazone induced a trabecular bone loss (Fig. 4*A*) with a significant reduction in BV/TV (−58%), BS (−54%), Conn. D. (−65%), Tb.N (−42%), and Tb.Th (−28%), accompanied by a significant increase in Tb.Sp (+79%) (Fig. 4*B*). In contrast, rosiglitazone-induced bone loss was completely abolished in the FGF21-KO mice (Fig. 4 *A* and *B*). Bone marker ELISA analyses revealed that in WT mice, the rosiglitazone-induced bone loss was caused by a combination of decreased bone formation (−17% in PINP) (Fig. 4*C*) and increased bone resorption (+21% in CTX-1) (Fig. 4*D*). These rosiglitazone-induced bone marker changes were alleviated in the FGF21-KO mice (Fig. 4 *C* and *D*). Histomorphometry showed that in WT mice, rosiglitazone reduced the number of osteoblasts (Fig. 4 *E* and *F*), but increased the number of osteoclasts (Fig. 4 *G* and *H*) and adipocytes (Fig. 4 *I* and *J*). Again, these rosiglitazone-induced changes were largely absent in the FGF21-KO mice (Fig. 4 *E*–*J*). The difference between the complete block of rosiglitazone-induced bone loss in vivo (Fig. 4) and the partial block of rosiglitazone-induced adipogenesis marker genes in vitro (Fig. 3*G*) by FGF21 deletion may be due to a higher effective local rosiglitazone concentration in vitro (1 μM) than in vivo (oral gavage at 10 $mg \cdot kg^{-1} \cdot d^{-1}$ for 2 wk). Moreover, additional systemic factors that were absent in the in vitro cultures could modulate the effects of FGF21 deletion in vivo. Together, these data provide compelling evidence that FGF21 enhances PPAR-γ activity in bone and represents a critical mediator of rosiglitazone-induced bone loss (Fig. 4*K*).

In summary, this work reveals FGF21 as a negative regulator of bone. Mechanistically, FGF21 forms a feed-forward loop to mediate and enhance PPAR-γ activity, thereby potentiating the ability of PPAR-γ agonist to inhibit osteoblastogenesis and stimulate adipogenesis from bone marrow MSCs. Consequently, FGF21 deletion confers resistance to rosiglitazone-induced bone loss (Fig. 4*K*). Importantly, our results suggest that, despite the beneficial effects of FGF21 in treating insulin resistance and type 2 diabetes, long-term FGF21 administration may cause skeletal fragility. Future studies are needed to determine whether FGF21 also promotes bone loss in human diabetic patients. Finally, the finding that the metabolic hormone FGF21 is a key regulator of bone homeostasis not only underscores the importance of whole-body energy metabolism in bone physiology, but also highlights the endocrine FGF hormones as a unique family of skeletal modulators that comprise both the previously described FGF23/Klotho axis (40, 41) and the newly identified FGF21/β-Klotho axis.

Materials and Methods

Mice. FGF21-Tg and FGF21-KO mice have been described (13, 31). Mice were fed standard chow containing 4% fat ad libitum unless stated otherwise. For diet-induced obesity, mice were fed a high-fat diet containing 60% of kilocalories from fat (Research Diets no. D12492). All animal experiments were approved by the Institutional Animal Care and Use Committee of the University of Texas Southwestern Medical Center.

Bone Analyses. μCT and static histomorphometry were performed as described (39). ORO staining of adipocytes was performed as described (42). Dynamic histomorphometry was performed as described (38, 43). PINP and CTX-1 were measured with a Rat/Mouse PINP EIA kit and a RatLaps EIA kit (Immunodiagnostic Systems), respectively.

Pharmacological FGF21 Treatment. Recombinant human FGF21 (residues 29–209) was expressed and purified as described (10). For in vivo treatment, WT mice were fed a high-fat diet for 4 mo and i.p. injected with FGF21 (1 $mg \cdot kg^{-1} \cdot d^{-1}$) or PBS control during the last 2 wk. Mice were euthanized 1.5 h after the final injection. For ex vivo treatment, bone marrow cells were differentiated in the presence of FGF21 (0.2 μg/mL) or PBS control.

Ex Vivo Bone Marrow Differentiation. Osteoblasts were differentiated from marrow MSCs as described (43–45). Briefly, cells were cultured for 3–7 d in MSC medium (Mouse MesenCult Proliferation Kit; StemCell Technologies), then differentiated in α-MEM containing 10% FBS, 5 mM β-glycerophosphate, and 100 μg/mL ascorbic acid (mineralization medium) (GPAA mixture) for 9 d. Mature osteoblasts were identified as ALP^+ cells by using fast red violet LB salt. For adipocyte differentiation, bone marrow cells were cultured for 3–7 d in MSC medium and differentiated in α-MEM containing 10% FBS, dexamethasone (1 μM), 3-isobutyl-1-methylxanthine (IBMX; 0.5 mM), and insulin (5 μg/mL) (DMI mixture) for 2 d and then in α-MEM containing 10% FBS and insulin (5 μg/mL) for an additional 4 d. Mature adipocytes were identified as ORO^+ cells. Osteoclasts were differentiated as described (38, 39).

Immunoprecipitation Analyses. Bone marrow cells from FGF21-KO mice were differentiated into adipocytes in the presence of rosiglitazone (1 μM) and then treated with rFGF21 (0.2 μg/mL) or vehicle control for 4 h. Whole-cell extract was immunoprecipitated with anti-Sumo-1 (Santa Cruz), and the elute was immunoblotted with anti–PPAR-γ (Cell Signaling). Input cell extract was immunoblotted with anti–PPAR-γ or anti–β-actin (Sigma).

Statistical Analyses. All statistical analyses were performed with Student's *t* test and presented as mean ± SD. The *P* values were designated as follows: $*P < 0.05$; $**P < 0.01$; $***P < 0.005$; $****P < 0.001$; n.s. nonsignificant ($P > 0.05$).

ACKNOWLEDGMENTS. We thank members of our laboratories for helpful discussion. Y.W. is a Virginia Murchison Linthicum Scholar in Medical Research. D.J.M. is an investigator for the Howard Hughes Medical Institute. This work was supported by the University of Texas Southwestern Endowed Scholar Startup Fund (Y.W.); Cancer Prevention and Research Institute of Texas Grant RP100841 (to Y.W.); March of Dimes Grant 5-FY10-1 (to Y.W.); Welch Foundation Grants I-1751 (to Y.W.), I-1275 (to D.J.M.), and I-1558 (to S.A.K.); National Institutes of Health (NIH) Grants R01DK089113 (to Y.W.), RL1GM084436 and R56DK089600 (to D.J.M. and S.A.K.), and U19DK062434 (to D.J.M.); NIH Predoctoral Training Grants GM007062 (to A.L.B.) and DE13686 (to M.M.); and the Howard Hughes Medical Institute (D.J.M.).

1. Canalis E, Giustina A, Bilezikian JP (2007) Mechanisms of anabolic therapies for osteoporosis. *N Engl J Med* 357:905–916.
2. Rachner TD, Khosla S, Hofbauer LC (2011) Osteoporosis: Now and the future. *Lancet* 377:1276–1287.
3. Zaidi M (2007) Skeletal remodeling in health and disease. *Nat Med* 13:791–801.
4. Akune T, et al. (2004) PPARgamma insufficiency enhances osteogenesis through osteoblast formation from bone marrow progenitors. *J Clin Invest* 113:846–855.
5. Karsenty G, Kronenberg HM, Settembre C (2009) Genetic control of bone formation. *Annu Rev Cell Dev Biol* 25:629–648.
6. Kawai M, Rosen CJ (2010) PPARγ: a circadian transcription factor in adipogenesis and osteogenesis. *Nat Rev Endocrinol* 6:629–636.
7. Lazarenko OP, et al. (2007) Rosiglitazone induces decreases in bone mass and strength that are reminiscent of aged bone. *Endocrinology* 148:2669–2680.
8. Pittenger MF, et al. (1999) Multilineage potential of adult human mesenchymal stem cells. *Science* 284:143–147.
9. Novack DV, Teitelbaum SL (2008) The osteoclast: Friend or foe? *Annu Rev Pathol* 3: 457–484.
10. Goetz R, et al. (2007) Molecular insights into the klotho-dependent, endocrine mode of action of fibroblast growth factor 19 subfamily members. *Mol Cell Biol* 27: 3417–3428.
11. Itoh N, Ornitz DM (2008) Functional evolutionary history of the mouse Fgf gene family. *Dev Dyn* 237:18–27.
12. Badman MK, et al. (2007) Hepatic fibroblast growth factor 21 is regulated by PPAR-alpha and is a key mediator of hepatic lipid metabolism in ketotic states. *Cell Metab* 5:426–437.
13. Inagaki T, et al. (2007) Endocrine regulation of the fasting response by PPARalpha-mediated induction of fibroblast growth factor 21. *Cell Metab* 5:415–425.
14. Lundåsen T, et al. (2007) PPARalpha is a key regulator of hepatic FGF21. *Biochem Biophys Res Commun* 360:437–440.
15. Dutchak PA, et al. (2012) Fibroblast growth factor-21 regulates PPARgamma activity and the antidiabetic actions of thiazolidinediones. *Cell*, 10.1016/j.cell.2011.11.062.
16. Muise ES, et al. (2008) Adipose fibroblast growth factor 21 is up-regulated by peroxisome proliferator-activated receptor gamma and altered metabolic states. *Mol Pharmacol* 74:403–412.
17. Wang H, Qiang L, Farmer SR (2008) Identification of a domain within peroxisome proliferator-activated receptor gamma regulating expression of a group of genes containing fibroblast growth factor 21 that are selectively repressed by SIRT1 in adipocytes. *Mol Cell Biol* 28:188–200.
18. Zhang X, et al. (2008) Serum FGF21 levels are increased in obesity and are independently associated with the metabolic syndrome in humans. *Diabetes* 57: 1246–1253.
19. Berglund ED, et al. (2009) Fibroblast growth factor 21 controls glycemia via regulation of hepatic glucose flux and insulin sensitivity. *Endocrinology* 150:4084–4093.
20. Coskun T, et al. (2008) Fibroblast growth factor 21 corrects obesity in mice. *Endocrinology* 149:6018–6027.
21. Kharitonenkov A, et al. (2005) FGF-21 as a novel metabolic regulator. *J Clin Invest* 115: 1627–1635.
22. Kharitonenkov A, et al. (2007) The metabolic state of diabetic monkeys is regulated by fibroblast growth factor-21. *Endocrinology* 148:774–781.
23. Xu J, et al. (2009) Fibroblast growth factor 21 reverses hepatic steatosis, increases energy expenditure, and improves insulin sensitivity in diet-induced obese mice. *Diabetes* 58:250–259.
24. Grey A (2009) Thiazolidinedione-induced skeletal fragility—mechanisms and implications. *Diabetes Obes Metab* 11:275–284.
25. Strotmeyer ES, Cauley JA (2007) Diabetes mellitus, bone mineral density, and fracture risk. *Curr Opin Endocrinol Diabetes Obes* 14:429–435.
26. Home PD, et al.; RECORD Study Team (2009) Rosiglitazone evaluated for cardiovascular outcomes in oral agent combination therapy for type 2 diabetes (RECORD): a multicentre, randomised, open-label trial. *Lancet* 373:2125–2135.
27. Kahn SE, et al.; ADOPT Study Group (2006) Glycemic durability of rosiglitazone, metformin, or glyburide monotherapy. *N Engl J Med* 355:2427–2443.
28. Kahn SE, et al.; Diabetes Outcome Progression Trial (ADOPT) Study Group (2008) Rosiglitazone-associated fractures in type 2 diabetes: An analysis from a diabetes outcome progression trial (ADOPT). *Diabetes Care* 31:845–851.
29. Zinman B, et al.; ADOPT Study Group (2010) Effect of rosiglitazone, metformin, and glyburide on bone biomarkers in patients with type 2 diabetes. *J Clin Endocrinol Metab* 95:134–142.
30. Inagaki T, et al. (2008) Inhibition of growth hormone signaling by the fasting-induced hormone FGF21. *Cell Metab* 8:77–83.
31. Potthoff MJ, et al. (2009) FGF21 induces PGC-1alpha and regulates carbohydrate and fatty acid metabolism during the adaptive starvation response. *Proc Natl Acad Sci USA* 106:10853–10858.
32. Nakashima T, et al. (2011) Evidence for osteocyte regulation of bone homeostasis through RANKL expression. *Nat Med* 17:1231–1234.
33. Xiong J, et al. (2011) Matrix-embedded cells control osteoclast formation. *Nat Med* 17:1235–1241.
34. Ali AA, et al. (2005) Rosiglitazone causes bone loss in mice by suppressing osteoblast differentiation and bone formation. *Endocrinology* 146:1226–1235.
35. Li M, et al. (2006) Surface-specific effects of a PPARgamma agonist, darglitazone, on bone in mice. *Bone* 39:796–806.
36. Sottile V, Seuwen K, Kneissel M (2004) Enhanced marrow adipogenesis and bone resorption in estrogen-deprived rats treated with the PPARgamma agonist BRL49653 (rosiglitazone). *Calcif Tissue Int* 75:329–337.
37. Wan Y (2010) PPARγ in bone homeostasis. *Trends Endocrinol Metab* 21:722–728.
38. Wan Y, Chong LW, Evans RM (2007) PPAR-gamma regulates osteoclastogenesis in mice. *Nat Med* 13:1496–1503.
39. Wei W, et al. (2010) PGC1beta mediates PPARgamma activation of osteoclastogenesis and rosiglitazone-induced bone loss. *Cell Metab* 11:503–516.
40. ADHR Consortium (2000) Autosomal dominant hypophosphataemic rickets is associated with mutations in FGF23. *Nat Genet* 26:345–348.
41. Shimada T, et al. (2004) Targeted ablation of Fgf23 demonstrates an essential physiological role of FGF23 in phosphate and vitamin D metabolism. *J Clin Invest* 113:561–568.
42. Wan Y, et al. (2007) Maternal PPAR gamma protects nursing neonates by suppressing the production of inflammatory milk. *Genes Dev* 21:1895–1908.
43. Wei W, et al. (2011) Biphasic and dosage-dependent regulation of osteoclastogenesis by β-catenin. *Mol Cell Biol* 31:4706–4719.
44. Wei W, et al. (2011) Osteoclast progenitors reside in the peroxisome proliferator-activated receptor γ-expressing bone marrow cell population. *Mol Cell Biol* 31: 4692–4705.
45. Krum SA, et al. (2008) Estrogen protects bone by inducing Fas ligand in osteoblasts to regulate osteoclast survival. *EMBO J* 27:535–545.